DSMC Simulation of Shock/Shock Interactions: Emphasis on Type IV Interactions

J.N. Moss[1], T. Pot[2], B. Chanetz[2], M. Lefebvre[2]

1. NASA Langley Research Center, Hampton, VA, 23681-2199, USA
2. ONERA, 92322 Châtillon, FRANCE

Abstract: This paper presents the results of a numerical study of shock/shock interactions that include both the Edney type IV and type III interactions, with emphasis on the type IV interactions. Computations are made using the direct simulation Monte Carlo (DSMC) method of Bird for Mach 10 air flow, as produced in the ONERA R5Ch low-density wind tunnel. The simulations include the flow about a shock generator which creates a relatively weak oblique shock that impinges on a much stronger cylinder bow shock. The sensitivity and characteristics of the interactions are examined by varying the horizontal distance separating the shock generator leading edge and cylinder. Results of the simulation for one separation distance are compared with wind tunnel measurements. Comparisons are made for surface heating and pressure and for flow-field values of density and rotational temperatures, as obtained with the Dual-line Coherent Anti Stokes Scattering (DL-CARS) technique. The comparisons between experiment and calculation yield a consistent description of the shock interaction features and a consistent description of the surface heating and pressure distributions, with the exception of the peak values–the computed values being greater than the measured values.

Key words: DSMC simulations, shock/shock interactions, nonintrusive measurements, DL-CARS, low density, hypersonic, type IV, and type III interactions

1. Introduction

Shock/shock and shock/boundary-layer interactions play a significant role in hypersonic flows because of the presence of intense shock waves which can strongly affect vehicle aerodynamic performance and lead to substantial localized aerothermal loads. For many hypersonic vehicles, the prospect of augmented aerothermal loads resulting from such interactions is unavoidable; therefore, techniques which accurately predict the magnitude of the surface heating are required for vehicle design.

In the present study, results of numerical simulations for Mach 10 air are presented for a range of shock-interaction patterns that encompass both the Edney (1968) type III and type IV interactions. One of the type IV conditions investigated numerically has also been investigated experimentally in the ONERA R5Ch hypersonic wind tunnel by Pot et al. (1998) and serves as the primary focus in the current study. Furthermore, this experimental test condition served as one of the test cases for the First Eastern-Western High Speed Flow Fields Conference and Workshop, Kyoto, Japan, November 1998. The interaction patterns are developed by impinging a relatively weak oblique shock on a much stronger bow shock produced by a 0.016-m-diameter cylinder. The flow in the interaction region is laminar because the tests are conducted at low Reynolds number ($\mathrm{Re}_{\infty,d} = 2658$) conditions. Also, the flow is assumed to be steady, as has been corroborated by the time-accurate Navier-Stokes calculations of Glass (1999). The current calculations are made by using the direct simulation Monte Carlo (DSMC) method of Bird (1992), where the simulated flow domain encompasses both the shock generator and cylinder. The current computational investigation benefits from the experience of Carlson and Wilmoth (1992), where the DSMC method was first applied to the type IV shock-interaction problem. The current two-dimensional simulations are for free-stream conditions of 1450 m/s velocity, 3.9×10^{-4} kg/m^3 density, and 52.5 K temperature.

2. Problem specification

An experimental test program has been conducted (Pot et al. (1998)) by France's Office National d'Etudes et de Recherches Aérospatiales (ONERA) to investigate shock/shock interactions induced by an oblique shock impinging on the bow shock of a cylinder. Figure 1 presents a schematic of the test model(s), with dimensions given in mm. The experiments were conducted in the ONERA R5Ch wind tunnel with a contoured nozzle that provided a uniform, free-stream environment with a diameter of 0.2 m. The nominal stagnation conditions for the tests were 2.5 bars and 1050 K, which provided free-stream air flow properties of $M_\infty = 10$, $T_\infty = 52.5\,\mathrm{K}$, $p_\infty = 5.9$

Pa, and $Re_\infty/m = 1.66 \times 10^5$. The viscosity ($3.405 \times 10^{-6}$ Pa·s) is that given by the Sutherland expression. The Reynolds number, based on the cylinder diameter (0.016 m), is 2658.
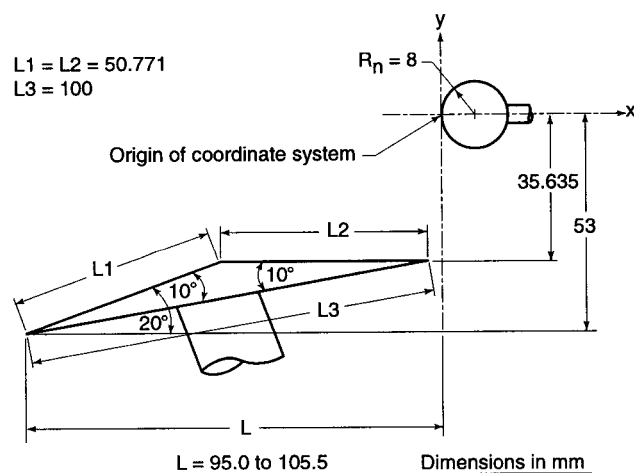

L1 = L2 = 50.771
L3 = 100

$R_n = 8$

Origin of coordinate system

35.635

53

10°
10°
20°

L1
L2
L3

L

L = 95.0 to 105.5

Dimensions in mm

Figure 1. Configuration for ONERA shock/shock interaction experiment.

The shock generator (Fig. 1) cross section is an isosceles triangle. Both the base length L3 and spanwise dimensions are 0.1 m. The leading-edge angle is 10°. The shock generator is rotated 10° into the flow such that one side appears as a 20° wedge to the free stream. In this position, the other equal length side is parallel to the free-stream flow. The leading edge of the shock generator is positioned at a distance L upstream of the cylinder and 0.053 m below the axis of the cylinder. The cylinder diameter is 0.016 m and the spanwise dimension is 0.1 m. The cylinder spanwise length to diameter ratio is 6.25 and should be sufficient to produce two-dimensional flow in the middle of the cylinder, the location where the surface measurements are made.

The DSMC code used in the current study is the general 2D/axisymmetric code of Bird (1992). The molecular collisions are simulated by using the variable hard sphere (VHS) molecular model. Energy exchange between kinetic and internal modes is controlled by the Larsen-Borgnakke (1975) statistical model. For the present study, the simulations are performed by using a nonreacting gas model consisting of two species while considering energy exchange between translational, rotational, and vibrational modes. A rotational relaxation collision number of 5 was used for the calculations. The vibrational collision number was 50. The reference conditions for the VHS model were as follows: reference temperature = 300 K, temperature exponent of the viscosity coefficient = 0.75, and reference diameters for O_2 and N_2 were 3.96×10^{-10} m and 4.07×10^{-10} m, respectively. The model surfaces are

assumed to have a temperature of 300 K. Full thermal accommodation and diffuse reflection are assumed for the gas-surface interactions.

3. Results and discussion

3.1. Undisturbed flow about cylinder

Only a brief summary of the results for the undisturbed cylinder is given. The calculation was made with a three-region computational domain following a grid resolution and time step sensitivity study. Results indicated that the surface and flow-field results were no longer influenced by additional refinement of either of these two key numerical parameters. The bow shock detachment location along the stagnation streamline is 3.1 mm upstream (maximum density gradient in shock wave) of the cylinder, or a value of 0.39, when normalized with the nose radius. Along the axis of symmetry, the shock wave is about 0.6 mm thick and exhibits thermal nonequilibrium. For most of the shock layer, however, the rotational and translational temperatures are in equilibrium. The calculated stagnation-point heating-rate value is 5.7 W/cm^2 and the corresponding surface pressure is 760 Pa. Figure 2 presents the calculated surface heating distribution and the experimental measurements. The heating rate measurement technique employed is the "thick skin" method described by Pot et al. (1998). The agreement between calculation and experiment is generally good.
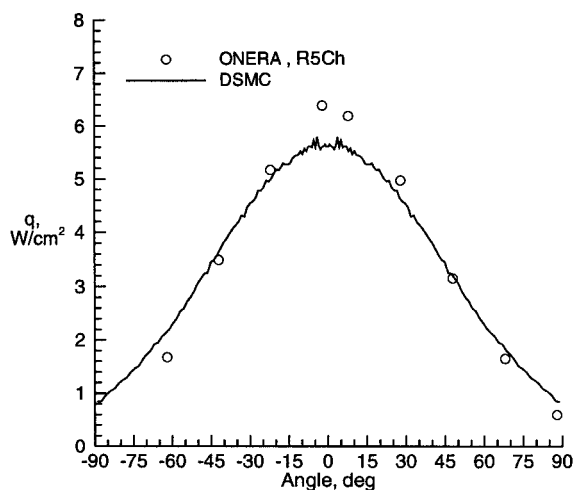

Figure 2. Cylinder heating-rate distributions.

3.2. Shock/shock interactions

Data presented in Figs. 3-13 are for interacting flows and provide insight to the sensitivity of the DSMC calculations to grid resolution and heating and pressure augmentations due to a type IV interaction. Also dis-

cussed are comparisons with measurements, details of the flow structure with corroborating data from DL-CARS measurements, and the sensitivity of heating and pressure distributions to the horizontal separation distance (7 values) between shock generator and cylinder.
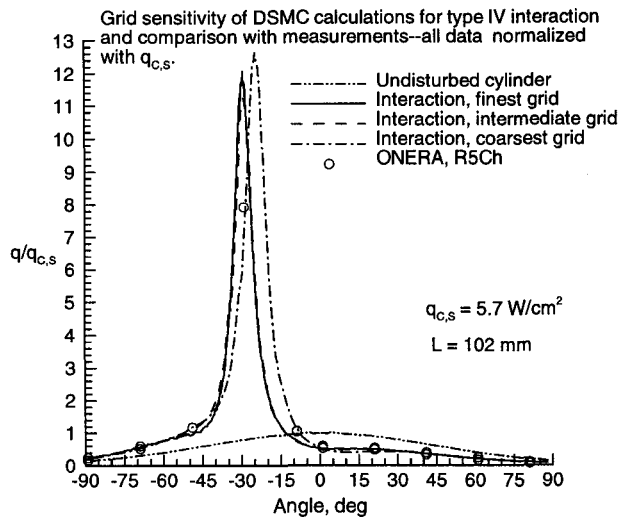

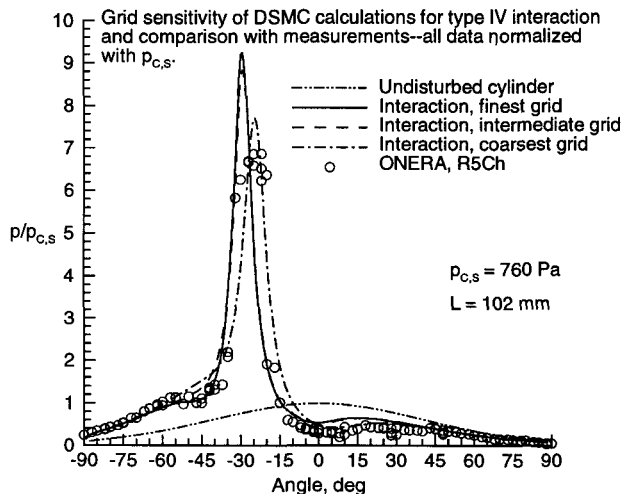
Figure 3. Nondimensional heating-rate distributions.

Figure 4. Nondimensional pressure distributions.

Results of the grid sensitivity investigation are summarized in Figs. 3-4 where the effect on surface heating and pressure distributions are shown, respectively. Data for three different body-fitted grids are presented. For each of the three grids, the overall computational domain is subdivided into 13 arbitrary regions. (Within a region, the time step and scale factor relating the number of simulated

molecules to the number of real molecules are constants.) The grid adjustments consisted of minor regional boundary adjustments with substantial alterations in the number of cells and time steps for the regions containing the shock triple points, transmitted shock, and jet impingement. Options available for stretching the grid in both directions were used extensively, as were subcells–subdividing cells into smaller units to provide much of the cell refinement benefits at a reduced computational overhead, as compared with increasing the number of cells. The number of cells/subcells used for the three grids are as follows: coarsest—29,200/116,800, intermediate—63,510/254,040, and finest—97,060/958,490. Also, the computational time step was reduced as the grid was refined. For the finest grid, the regional time steps ranged from 1.2 to 9.0 ns. The computational refinement had a very noticeable effect on both location (shift from -24.3° to -29°) and magnitude of peak heating and pressure as the adjustments were made between the coarsest and intermediate conditions. For the intermediate and finest grid simulation parameters, the calculated surface results are in good agreement. The calculated augmentation factors (peak values divided by undisturbed cylinder stagnation values) for heating and pressure are 12.1 and 9.2, respectively. All computational data presented are time-averaged results. For the finest grid and L=102 mm, the simulation consisted of 1.56×10^5 time steps to ensure steady state conditions, followed by an additional 46,000 time steps in which the time averaged data were accumulated.

Included in Figs. 3–4 are the results of experimental measurements—heating rates determined by using the "thick skin" method and pressure by employing differential sensors, as discussed by Pot et al. (1998). The trends of the experimental and computational data sets are consistent but with some differences in magnitude and location of peak quantities. Otherwise, along the wings of the peak values, the two data sets are in reasonably good agreement—very good for heating. The experimental heating data set does not have adequate spatial resolution to define the peak value; however, the pressure data set is more extensive and the peak value is located near -25° with a magnitude equal to ≈ 76% of the calculated value.

Figures 5–10 present information describing the flow-field structure for the type IV interaction where L=102 mm. As previously mentioned, the computational domain includes the shock generator and cylinder. Consequently, the simulation should provide, in principal, a high fidelity simulation of the experiment since the simulation accounts for displacement and expansion effects of the shock generator on the strength and curvature of the incident oblique shock. Over-

all flow-field features are demonstrated with the density contours presented in Fig. 5, demonstrating the type IV interaction. Enlarged views of the interaction features are shown in Figs. 6 and 7 for density and Mach contours, respectively. Evident are the two shock triple points, transmitted shock, and a clearly defined supersonic jet and its associated shear layers. The termination of the supersonic jet occurs very close to the surface—a distance from the surface equal to about 0.6 mm. Near the jet impingement point, the overall kinetic temperature is 1050 K. At the impingement point, -29° below the horizontal, the maximum density is 183 times the free-stream value and the maximum heating and pressure are 69 W/cm² and 7032 Pa, respectively.

Figure 7. Mach contours and streamlines.
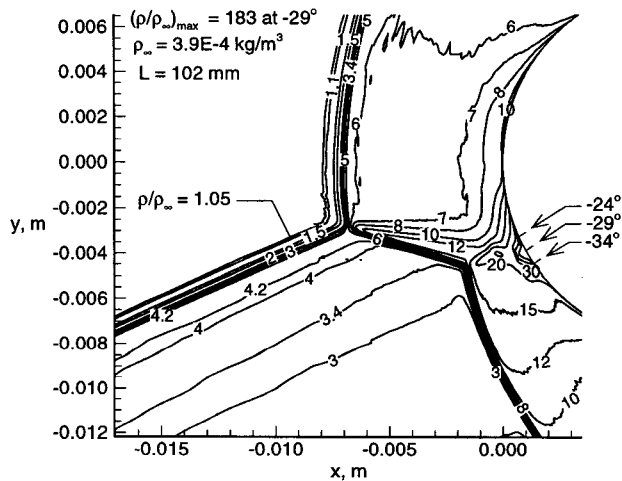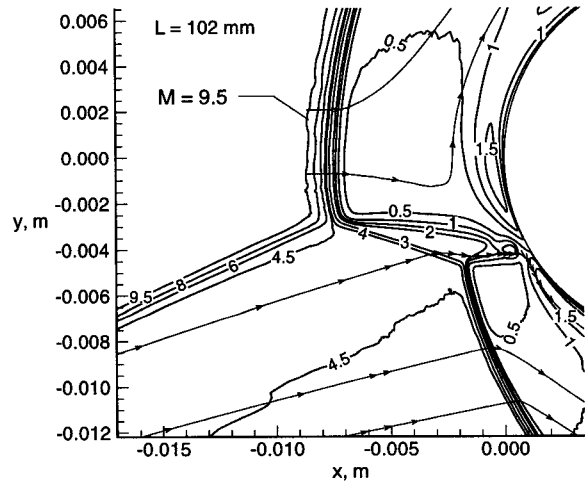
Characteristic of the type IV interaction is a large alteration in the undisturbed cylinder bow-shock location and configuration. This alteration is evident in the current case since the bow shock with interaction is 2.3 times thicker than the undisturbed case of 3.1 mm at y=0.
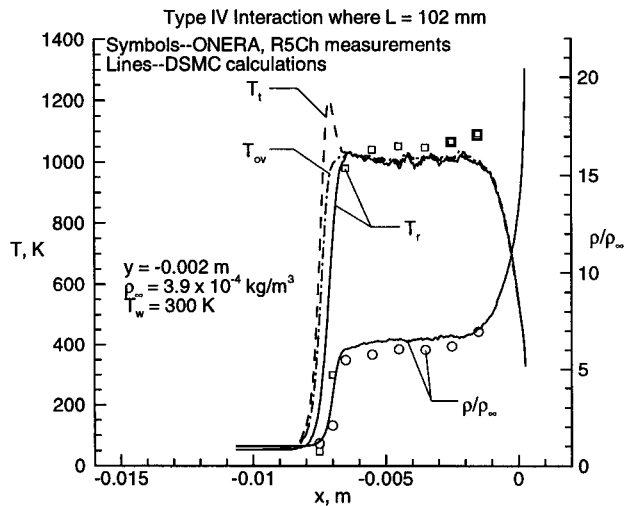

Figure 5. Nondimensional density contours.

Figure 8. Profiles at y = -2 mm.

Additional data describing the type IV interaction features are presented in Figs. 8–10, where horizontal profiles for density and temperature are shown for both the DSMC calculation and the ONERA DL-CARS measurements. The experimental data set consists of nine horizontal cuts at y-locations of 0 to -5 mm, with the minimum Δy spacing equal to 0.5 mm. Because of space limitations, only three horizontal pro-

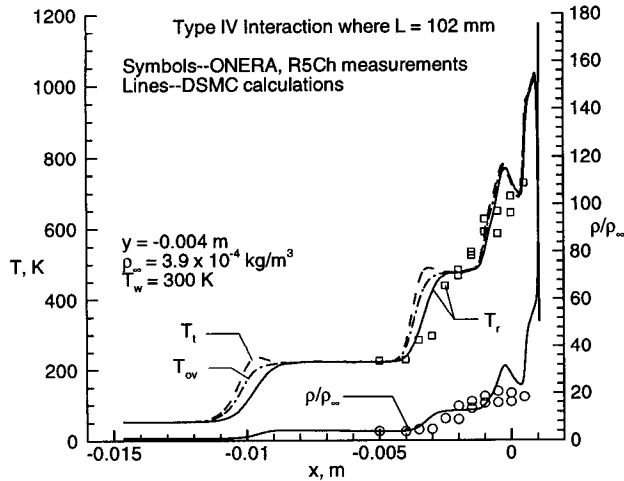**Figure 6.** Density contours in interaction region.
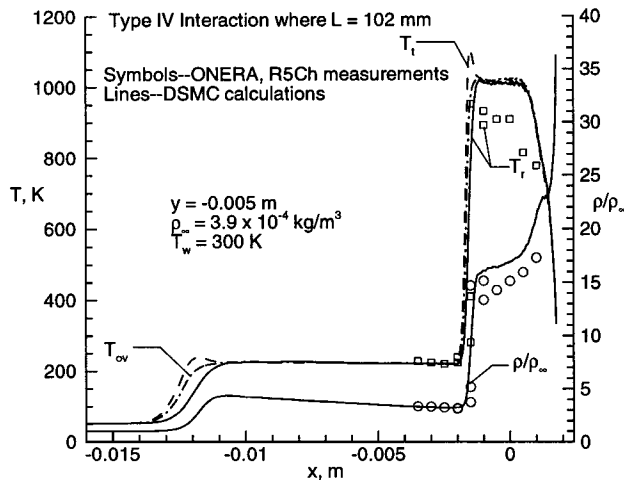
Figure 9. Profiles at y = -4 mm.

Figure 10. Profiles at y = -5 mm.

files are presented—one located above the upper shock triple point at y = -2 mm (Fig. 8), one that crosses the transmitted shock and intersects the surface one degree below jet impingement at y = -4 mm (Fig. 9), and one located just below the second triple point at y = -5 mm (Fig. 10). Comparison of the experimental and calculated profiles shows very good agreement in the bow shock, transmitted shock, and extended bow shock locations. Also, the trends of rotational temperature and density are consistent. The calculated temperature profiles presented are those for translational (T_t), rotational (T_r), and overall kinetic (T_{ov}) temperatures. (The overall kinetic temperature is a weighted mean of the translational and internal temperatures.) Evident is the extent of thermal nonequilibrium in the shock crossings and, for the most part,

equilibrium post-shock conditions. In Fig. 9, for example, one can see the changes that occur as the flow traverses the relatively weak oblique shock (near x = -10 mm) produced by the shock generator, followed by the crossing of the transmitted shock near x = -3.5 mm, and then the complex interactions in the jet impingement region—high temperatures near the surface and the density adjacent to the surface equal 178 times free stream.
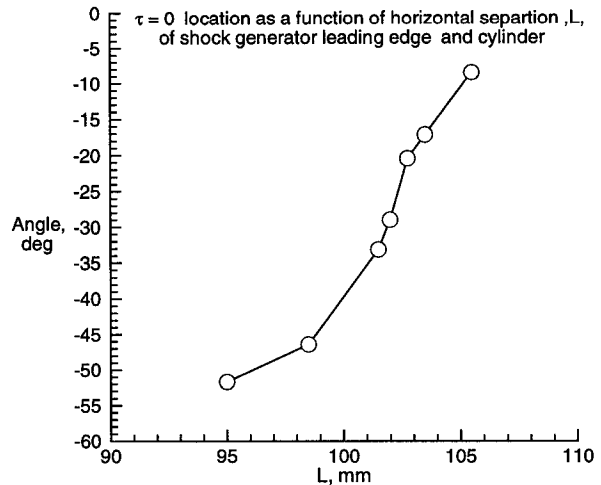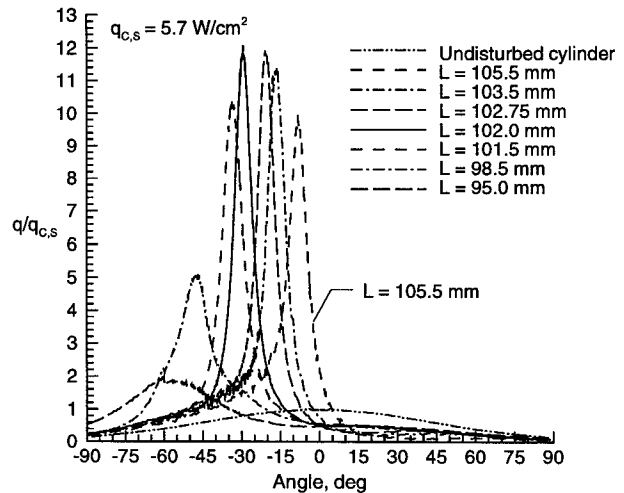

Figure 11. Location of zero shear stress.

Figure 12. Calculated heating-rate distributions.

The spatially resolved DL-CARS measurements for N_2 (air properties inferred from N_2 measurements) provide simultaneous values for rotational temperature and density. The signal is obtained by passing three laser beams through a flow volume 40 mm
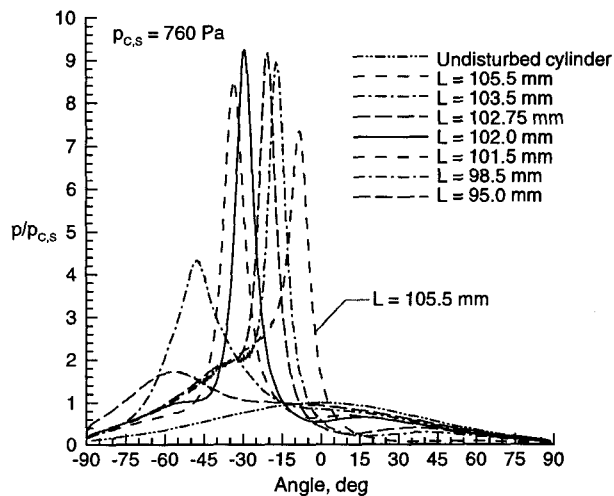
Figure 13. Calculated surface pressure distributions.

in length and 0.2 mm in diameter. The axis of the probe volume is oriented perpendicular to the free stream. Consequently, the spatial resolution in the strongest gradient direction is limited to 0.2 mm . A maximum of five spatial data points can be obtained during a R5Ch run, which has a maximum run duration of approximately one minute. Also, the signal is time averaged over a 9.6-second interval by taking 120 laser shots at a frequency of 12.5Hz. Basic fundamentals, including application issues of the DL-CARS technique, are discussed, for example, by Grisch et al. (1993). Additional details concerning the current DL-CARS measurements are given by Pot et al. (1998).

Figures 11–13 present data describing the sensitivity of the augmented surface heating and pressure conditions and their location as a function of horizontal separation distance (L varied between 95 and 105.5 mm—cylinder is downstream of wedge when L > 98.5 mm). The current calculations indicate that the maximum heating and pressure augmentations occur very close to an L separation of 102 mm, the focus of the current investigation. When one examines the data (Fig. 11) that shows the zero-shear-stress location (approximate location of maximum heating and pressure) as a function of L, the maximum slope (about 9 deg/mm) occurs near L = 102 mm. These results highlight the extreme precision that must be exercised when performing such experiments since a 1% change in L can produce a displacement in peak heating/pressure location on the order of 10°. The shock/shock interactions were type IV, with the exception of the two smaller values of L, which were type III interactions—interactions where the shear layer impacts the surface rather than a supersonic jet.

4. Concluding remarks

A numerical investigation is made of shock/shock interactions by using the direct simulation Monte Carlo method of Bird. The focus of this investigation is the Edney type IV interactions, as produced by an oblique shock interacting with the bow shock of a two-dimensional cylinder. The flow conditions simulated are those for which experiments have been conducted in the ONERA R5Ch low-density wind tunnel for Mach 10 air at a free-stream Reynolds number, based on cylinder diameter, of 2658. Sensitivity of the computed results to grid parameters and variations in the separation distance of the shock generator and cylinder are demonstrated. Comparisons of computed and measured results are made for surface heating and pressure and flow-field data for rotational temperature and density. The computational/experimental data demonstrate that the interactions are laminar. Furthermore, concerning the flow-field structure, the two data sets are in very good agreement. The peak heating rate and pressure values were found to have a single maximum as the horizontal separation of shock generator and cylinder was varied between 95 and 105.5 mm. The maximum augmentation factors calculated for heating and pressure were 12.1 and 9.2, respectively.

References

Edney B (1968) Anomalous heat transfer and pressure distributions on blunt bodies at hypersonic speeds in the presence of an impinging shock. Rep. 115, Flygtekniska Forsoksanstalten (The Aeronautical Research Institute of Sweden), Stockholm.

Pot T, Chanetz B, Lefebvre M, Bouchardy P (1998) Fundamental study of shock/shock interference in low density flow. Presented at the 21st International Symposium on Rarefied Gas Dynamics.

Glass CE (1999) Numerical simulation of low density shock-wave interactions. 20th International Symposium on Shock Waves: London, UK.

Bird GA (1992) The G2/A3 program users manual. G.A.B. Consulting Pty Ltd, Killara, N.S.W, Australia.

Carlson AB, Wilmoth RG (1992) Shock interference prediction using direct simulation Monte Carlo. Journal of Spacecraft and Rockets 29-6: 780–785

Borgnakke C, Larsen PS (1975) Statistical collision model for Monte Carlo simulation of polyatomic gas mixture. Journal of Computational Physics 18: 405–420

Grisch F, Bouchardy P, Pealat M, Chanetz B, Pot T, Coet MC (1993) Rotational temperature and density measurement in a hypersonic flow by dual line CARS. Applied Physics B 56: 14–20